

Chapter 4

Spurious velocity changes caused by temporal variations in ambient noise frequency content

This chapter has been published as:

Zhan, Z., V. C. Tsai, and R. W. Clayton (2013). Spurious velocity changes caused by temporal variations in ambient noise frequency content. *Geophys. J. Int.*, 194 (3): 1574-1581. doi: 10.1093/gji/ggt170

4.1 Abstract

Ambient seismic noise cross correlations are now being used to detect temporal variations of seismic velocity, which are typically on the order of 0.1%. At this small level, temporal variations in the properties of noise sources can cause apparent velocity changes. For example, the spatial distribution and frequency content of ambient noise have seasonal variations due to the seasonal hemispherical shift of storms. Here we show that if the stretching method is used to measure time shifts, then the temporal variability of noise frequency content causes apparent velocity changes due to the changes in both amplitude and phase spectra caused by waveform stretching. With realistic seasonal variations of frequency content in the Los Angeles Basin, our numerical tests produce about 0.05% apparent velocity change, comparable to what

Meier et al. (2010) observed in the Los Angeles Basin. We find that the apparent velocity change from waveform stretching depends on time windows and station-pair distances, and hence it is important to test a range of these parameters to diagnose the stretching bias. Better understanding of spatiotemporal noise source properties is critical for more accurate and reliable passive monitoring.

4.2 Introduction

Using seismic waves to monitor temporal velocity changes in the Earth provides important information about a variety of geophysical processes, including earthquake stress cycles (e.g., Niu et al., 2008), fault-zone damage and healing (e.g., Li et al., 1998; Vidale and Li, 2003; Peng and Ben-Zion, 2005; Peng and Ben-Zion, 2006), volcanic eruptions (e.g., Grêt et al., 2005), and fluid movement (e.g., Niu et al., 2003). Direct and coda waves from natural and active repeating sources have been used for different problems (e.g., Poupinet et al., 1984; Niu et al., 2003; Rubinstein et al., 2007; Niu et al., 2008; Wang et al., 2008). However, application of these active monitoring approaches is limited by the lack of continuous or frequent high-quality repeating sources. With the rapid progress of noise cross correlation methods in the last decade, a passive monitoring method using ambient seismic noise has become popular. The basic idea is that the noise cross-correlation function (NCF) between two stations converges toward the Green's function between the stations, which is the response at one station if a source is placed at the other station. This allows us to treat seismic stations as continuous virtual repeating sources. The temporal resolution is only limited by the time required to get converged/stable NCFs (Hadziioannou et al., 2009). This passive monitoring method has been widely applied in regions with volcanoes or major earthquakes to detect velocity changes before and after volcanic eruptions (e.g., Sens-Schonfelder and Wegler, 2006; Brenguier et al., 2008b; Duputel et al.,

2009), earthquakes (e.g., Brenguier et al., 2008a; Xu and Song, 2009; Zaccarelli et al., 2011; Minato et al., 2012) or slow slip events (Rivet et al., 2011). Using the passive monitoring method, Meier et al. (2010) detect seasonal velocity changes within the Los Angeles Basin (with higher velocities in summer than in winter) and suggest that two possible reasons are hydrological and/or thermoelastic variations. However, Tsai (2011) shows that neither of the two models is likely to explain the observed velocity variations.

The observed temporal velocity changes by passive monitoring are typically small, of the order of 0.1% (e.g., Brenguier et al., 2008a; Meier et al., 2010). Many technical factors including convergence and quality of the NCFs, spatiotemporal variability of noise sources, and method to compare waveforms can introduce potentially comparable bias. Clarke et al. (2011) show that a certain NCF signal-to-noise (SNR) threshold is required to make reliable measurements with <0.1% accuracy. Using laboratory experiments, Hadziioannou et al. (2009) demonstrate that passive monitoring does not require accurate reconstruction of the Green's functions, but instead only requires the relative stability of the background noise structure. Despite this relaxed constraint, passive monitoring can have problems because in real geophysical problems, the noise structure is usually highly variable. For example, due to the seasonal shift of storm activity between the northern and southern hemispheres, the spatial distribution of noise sources is also seasonal. Before and after major earthquakes or volcanic eruptions, there are usually significantly different levels of seismic activity (e.g., aftershocks and volcanic tremor), whose signals are hard to remove completely from ambient seismic noise before cross correlation. In past studies, their effects were usually evaluated by examining consistency between the positive and negative sides of the NCFs (e.g., Brenguier et al., 2008a) or over station pairs with different azimuths (e.g., Meier et al., 2010). In this paper, we concentrate on another largely ignored factor, the temporal variability of noise frequency content, which occurs at different time

scales. For example, seasonal or even multi-decadal variations in storm activity cause long-term variations in noise frequency content at a global scale (e.g., McNamara and Buland, 2004; Aster et al., 2008). Increased earthquake or volcanic/non-volcanic tremor activity can cause changes in frequency content at shorter time scales. For example, Duputel et al. (2009) report a drift of dominant frequency around periods of volcanic eruption due to increased volcanic tremor. However, the effect of variable frequency content on passive monitoring is still not well quantified.

The sensitivity of NCFs to seismic velocity is from travel time information contained in their phase spectra. Therefore methods that mix amplitude and phase spectra potentially cause biases in velocity due to variations in the amplitude spectrum. Since the passive monitoring method is the same as the active monitoring method after preparing the NCFs, most passive studies adopt the same waveform comparison methods such as the doublet method (also known as moving window cross spectral method, MWCS, Poupinet et al., 1984). The doublet method measures the travel time difference between two waveforms in each time window by fitting the phase differences in the frequency domain. Theoretically, as long as appropriate windowing functions are used, this approach separates the amplitude spectrum and phase spectrum before making the measurements, hence is likely less affected by the change of frequency content. In another recently proposed method, called the stretching method, the time axis on one waveform is stretched to achieve the best cross correlation with another waveform. The best-fitting stretching ratio is then taken as an estimate of the relative velocity change. Theoretical and laboratory work show that the stretching method is more stable to fluctuations in noise compared to the traditional doublet method (Hadziioannou et al. 2009), and it has started to be widely used in passive monitoring applications (e.g., Sens-Schonfelder and Wegler, 2006; Duputel et al., 2009; Meier et al., 2010; Minato et al., 2012). In this paper we concentrate on this methodology's bias due to changes in frequency content. In sec-

tion 4.3 we will first theoretically illustrate the stretching method's problem of mixing amplitude and phase information during waveform comparison. Then in section 4.4, as an example, we will show that realistic changes in NCF frequency content within the Los Angeles Basin could cause changes comparable to those observed by Meier et al. (2010). Lastly, we will discuss how to diagnose this bias.

4.3 The stretching method and the effect of variable NCF amplitude spectrum

4.3.1 Summary of the stretching method in time and frequency domains

The stretching method builds on the fact that the relative time shift between two waveforms due to a small uniform velocity change is proportional to the travel time. Suppose we have two NCFs, a reference NCF $u_r(t)$ and a current NCF $u_c(t)$, and we use the stretching method to measure the relative velocity change $\varepsilon_v = \delta v/v$. The stretching method will first stretch the current NCF assuming a relative velocity change of ε ,

$$u_c(t; \varepsilon) \equiv u_c(t(1 - \varepsilon)) \quad (4.1)$$

Then the stretched waveform $u_c(t; \varepsilon)$ is correlated with the reference waveform $u_r(t)$ in the time domain:

$$C(\varepsilon) = \frac{\int_{t_1}^{t_2} u_r(t)u_c(t; \varepsilon)dt}{\sqrt{\int_{t_1}^{t_2} u_r^2(t)dt \int_{t_1}^{t_2} u_c^2(t; \varepsilon)dt}} \quad (4.2)$$

where t_1 and t_2 define the time window. The stretching method grid-searches over ε to find the apparent velocity change ε_{max} that maximizes $C(\varepsilon)$ as an estimate of the

relative velocity change ε_v .

The above waveform stretching and correlation are usually conducted entirely in the time domain. However, to show how different amplitude spectra affect the measurement, here we restate the method in the frequency domain. Letting $U_r(\omega)$ and $U_c(\omega)$ to be the Fourier transforms of $u_r(t)$ and $u_c(t)$, respectively, then

$$U_r(\omega) = F\{u_r(t)\} = A_r(\omega)e^{i\varphi_r(\omega)} \quad (4.3)$$

$$U_c(\omega) = F\{u_c(t)\} = A_c(\omega)e^{i\varphi_c(\omega)} \quad (4.4)$$

where $A_r(\omega)$ and $A_c(\omega)$ are the amplitude spectra, $\varphi_r(\omega)$ and $\varphi_c(\omega)$ are the phase spectra. Taking the Fourier transform of Eq. (4.1), then waveform stretching in the frequency domain can be written as

$$U_c(\omega; \varepsilon) = \frac{1}{1-\varepsilon} U_c\left(\frac{\omega}{1-\varepsilon}\right) \approx (1+\varepsilon)U_c(\omega(1+\varepsilon)) = (1+\varepsilon)A_c(\omega(1+\varepsilon))e^{i\varphi_c(\omega(1+\varepsilon))} \quad (4.5)$$

where the approximation applies to $\varepsilon \ll 1$. Note that both the amplitude and phase spectra get stretched. For general dispersive waves with wavenumber k and propagation distance of x , we can further simplify the form of the phase spectrum:

$$\varphi(\omega(1+\varepsilon)) = k(\omega(1+\varepsilon)) \cdot x \approx kx + \frac{\partial k}{\partial \omega} \omega \varepsilon x = kx \left(1 + \frac{\omega \varepsilon}{kv_g}\right) = \varphi(\omega) \left(1 + \frac{c}{v_g} \varepsilon\right) \quad (4.6)$$

where c is phase velocity and v_g is group velocity. For non-dispersive waves $c = v_g$, and Eq. (4.6) simplifies to $\varphi(\omega(1+\varepsilon)) = \varphi(\omega)(1+\varepsilon)$. With the simplifications of Eq. (4.5) and (4.6) above, Eq. (4.2) showing the correlation of the reference waveform and stretched current waveform can be rewritten as:

$$\begin{aligned}
C(\varepsilon) &= \frac{\int_{-\infty}^{+\infty} U_r(\omega)U_c(\omega; \varepsilon)d\omega}{\sqrt{\int_{-\infty}^{+\infty} U_r^2(\omega)d\omega \int_{-\infty}^{+\infty} U_c^2(\omega; \varepsilon)d\omega}} \\
&= \frac{\int_{-\infty}^{+\infty} A_r(\omega)A_c(\omega(1 + \varepsilon))e^{i[\varphi_c(\omega(1+\varepsilon))-\varphi_r(\omega)]}d\omega}{\sqrt{\int_{-\infty}^{+\infty} A_r^2(\omega)d\omega \int_{-\infty}^{+\infty} A_c^2(\omega(1 + \varepsilon))d\omega}} \quad (4.7)
\end{aligned}$$

$C(\varepsilon)$ and ε_{max} depend on the forms of both the amplitude spectra $A_r(\omega)$, $A_c(\omega)$, and wave dispersions in the form of phase spectra $\varphi_r(\omega)$ and $\varphi_c(\omega)$.

4.3.2 Bias of the stretching method due to changes in the amplitude spectra

Since we are interested in the bias effect caused only by a variable amplitude spectrum, here we simplify $C(\varepsilon)$ by considering a special case that $u_r(t)$ and $u_c(t)$ have the same phase spectrum $\varphi(\omega)$ (i.e., no velocity variation). A stable measurement method should recover $\varepsilon_v = 0$ in this case. For this assumption, Equation (4.7) simplifies to

$$C(\varepsilon) = \frac{\int_{-\infty}^{+\infty} A_r(\omega)A_c(\omega(1 + \varepsilon))e^{i\frac{c}{v_g}\varepsilon\varphi(\omega)}d\omega}{\sqrt{\int_{-\infty}^{+\infty} A_r^2(\omega)d\omega \int_{-\infty}^{+\infty} A_c^2(\omega(1 + \varepsilon))d\omega}} \quad (4.8)$$

To decompose the effects of the amplitude and phase spectra, we first look at the result of the simplest non-dispersive case $\varphi(\omega) = 0$ so that $C(\varepsilon)$ is only controlled by the amplitude spectra $A_r(\omega)$ and $A_c(\omega)$:

$$C(\varepsilon) = \frac{\int_{-\infty}^{+\infty} A_r(\omega)A_c(\omega(1 + \varepsilon))d\omega}{\sqrt{\int_{-\infty}^{+\infty} A_r^2(\omega)d\omega \int_{-\infty}^{+\infty} A_c^2(\omega(1 + \varepsilon))d\omega}} \quad (4.9)$$

It is clear that the $C(\varepsilon)$ in this case is just the correlation function between the amplitude spectra $A_r(\omega)$ and stretched $A_c(\omega)$ in the frequency domain, which in general does not have $\varepsilon_{max} = 0$ under our assumption of variable frequency content, i.e. $A_r(\omega) \neq A(\omega)$. More generally, for the non-dispersive case, $\varphi(\omega) = \omega t_0$, we

calculate $\varepsilon_{max}(t_0)$ numerically, where t_0 is travel time of the wavelet. As an example, we assume that the reference $A_r(\omega)$ has a bell-shaped amplitude spectrum centered at 0.15 Hz and the current $A_c(\omega)$ has a stretched form of $A_r(\omega)$, and hence more high frequency energy, as shown in Figure 4.1A such that

$$A_c(\omega) = A_r\left(\frac{\omega}{1 + \varepsilon_0}\right) \quad (4.10)$$

where $\varepsilon_0 = 20\%$ and the resulting $\varepsilon_{max}(t_0)$ is displayed in Figure 4.1B. As discussed above, when $t_0 = 0$ s, $\varphi(\omega) = 0$, and ε_{max} is the same as the optimal stretching ratio of the amplitude spectra so $\varepsilon_{max} = \varepsilon_0 = 20\%$. $\varepsilon_{max}(t_0)$ decays rapidly when t_0 increases from 0 s due to the extra $i\frac{c}{v_g}\varepsilon\varphi(\omega)$ term in the integrand of $C(\varepsilon)$. However, up to $t_0 = 30$ s, the estimated ε_{max} is still of the order of 0.1%, comparable to the observed relative velocity changes in most real-data applications of the passive monitoring technique. Figure 4.1B also shows that the maximum cross-correlation coefficients $C(\varepsilon_{max})$ are all larger than 0.9, a general threshold for most real-data applications. This means that high cross correlation values do not guarantee reliable measurements. Figure 4.1C displays example reference and current waveforms for $t_0=20$ s, for which there is an apparent velocity increase of about 0.2%.

In this section, we have demonstrated that the stretching method changes the phase spectrum as well as the amplitude spectrum during measurements, and the amplitude spectrum contributes to the waveform correlation. This causes a bias in the estimate of the relative velocity change. In our simple synthetic tests where only the amplitude spectrum changes, the stretching method does not recover $\varepsilon_v = 0$, but instead produces systematic bias.

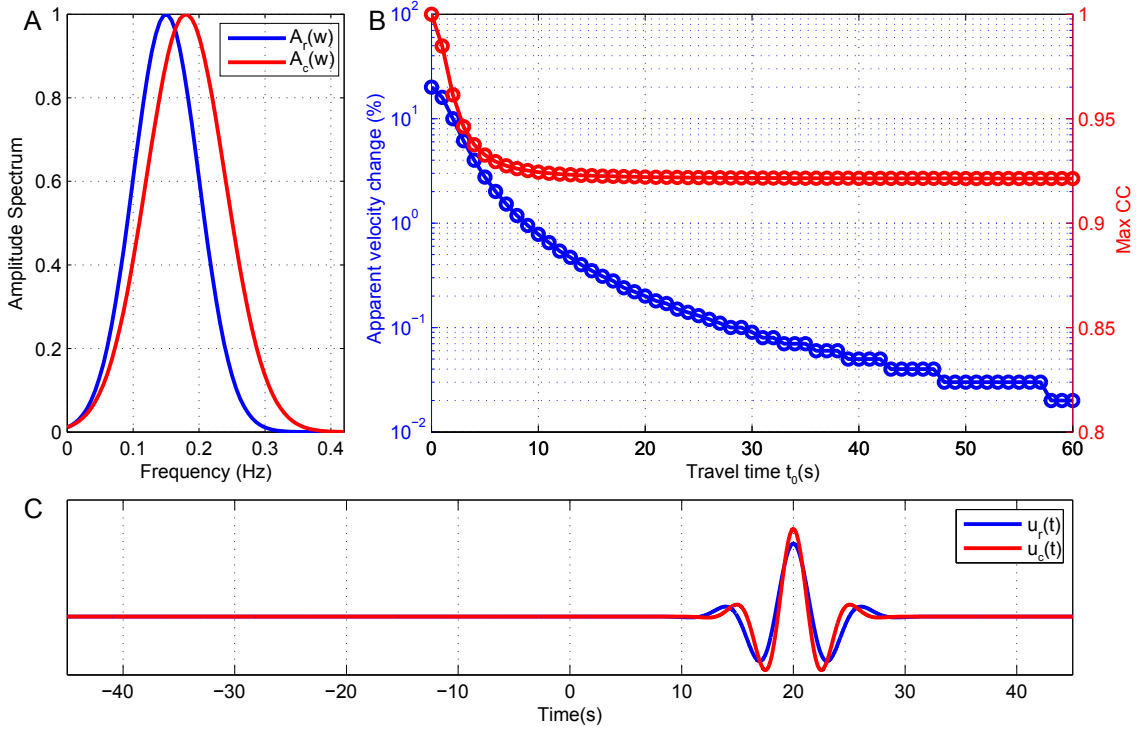


Figure 4.1: Numerical test of apparent velocity change $\varepsilon_{max}(t_0)$ caused by stretching of the NCF amplitude spectrum. (A) The reference NCF amplitude spectrum $A_r(\omega)$ has a Gaussian functional form with a center frequency of 0.15 Hz and $\sigma = 0.5$ Hz. The current NCF amplitude spectrum $A_c(\omega)$ is stretched from $A_r(\omega)$ by 20% to have more high frequency energy. (B) The blue line indicates the apparent velocity change $\varepsilon_{max}(t_0)$ calculated numerically using the stretching method. The red line shows the corresponding maximum cross correlation coefficients between the reference and current waveforms. Note that at $t_0 = 0$ s, the relative velocity change is 20%, the same as the stretching ratio between the input NCF amplitude spectra, and the maximum correlation value is 1.0. (C) Example waveforms of the reference NCF and current NCF at $t_0 = 20$ s, corresponding to a relative velocity change of about 0.2%.

4.4 Bias due to seasonal variation of noise frequency content in the Los Angeles Basin

Real ambient seismic noise and NCFs have more complicated temporal variations of frequency content than that discussed in section 4.3.2. In this section, we will use more realistic examples with data from the Los Angeles Basin to evaluate the bias caused by the frequency content change in the stretching method.

The frequency content of ambient noise at stations within USArray is now routinely calculated by IRIS for quality control of data. Raw noise spectra are calculated using the method of McNamara and Buland (2004) for overlapping half-hour windows throughout the day and presented as probability density functions (PDFs). Each day's power spectrum is the mode of the spectral values of the half-hour windows. Taking DEC, a broadband station at the edge of the LA basin as an example, we display its daily noise PDF between 2004 and 2011 in Figure 4.2A. The most obvious temporal variation in Figure 4.2A is the seasonal pattern, with stronger noise in winter and weaker noise in summer, probably caused by the seasonal hemispherical shift of storms (e.g., Stehly et al., 2006; Aster et al., 2008). Figure 4.2B shows the averaged power spectra for a whole year, winter only (December, January and February) and summer only (June, July and August), respectively. In addition to the absolute noise level changes, the shape of the spectrum also changes. For example, the differences between winter and summer in the power spectrum at $T < 4$ s are much less than those at $T \approx 8$ s.

In addition to being affected by the raw ambient noise levels, NCFs are also affected by a number of pre-processing steps. Here we follow common procedures (e.g., Bensen et al., 2007; Meier et al., 2010; Zhan et al., 2011) to calculate the NCF for station pair WTT-LCG inside the Los Angeles Basin as an example. We use continuous broadband vertical-component data from 2003 to 2011, remove instrumental

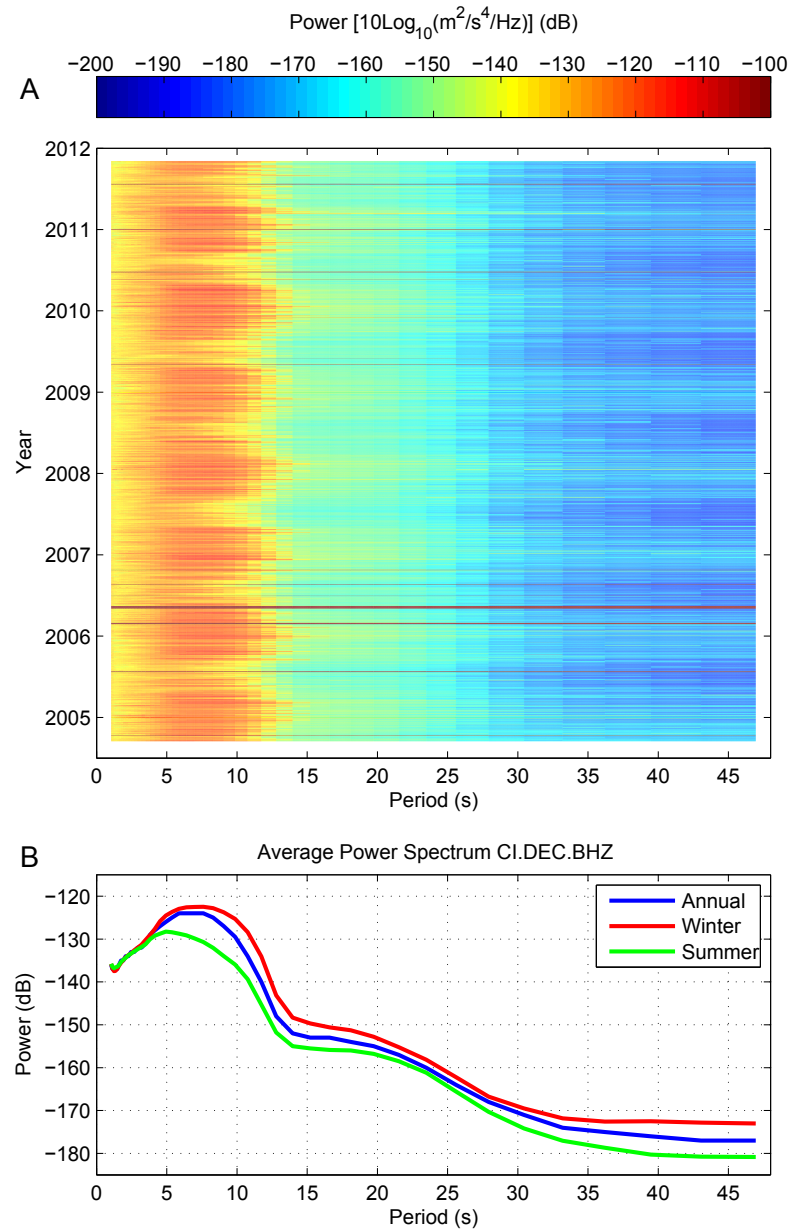


Figure 4.2: Temporal variability of raw noise frequency content. (A) Temporal variations in the noise power spectrum from 2004 to 2011 at station DEC. The dominant seasonal pattern shows higher noise level in winter and lower noise level in summer. Occasional dark red horizontal bands are due to gaps in data or instrument problems. (B) The blue line indicates the average noise power spectrum with the strongest peak at the secondary microseism period of 7 s. The red and green lines display the average spectra for winter and summer, respectively. Note that not only the absolute noise level changes, but the shape of the spectrum also changes.

responses and cut the data into one-hour segments. To remove the effect of earthquakes, we first filter the original seismograms between 15 s and 50 s to emphasize the surface waves of earthquakes and then calculate envelope functions. The inverse of these smoothed envelope functions multiply the corresponding seismograms to down-weight the earthquake signals. We also tested the effect of using one-bit normalization, and the resulting NCFs are similar in waveforms and spectra. We chose to present only the results for envelope weighting because its effect on waveforms is better understood than one-bit normalization. After envelope down-weighting, we then apply spectral whitening to broaden the frequency band of the NCFs. Finally, the two stations' waveforms are cross correlated at 1 hour intervals and stacked with a 60-day moving window and with an overlap of 30 days (Figure 4.3). Due to the shallow sediment layer in the Los Angeles Basin, the direct wave-train between the two stations can be as slow as 0.5 km/s (Figure 4.3A). The 60-day NCFs show high signal-to-noise ratios and good convergences, although small seasonal variability of the NCF waveforms is visible (Figure 4.3B). The amplitude spectra of the 60-day NCFs have even more obvious seasonal patterns (Figure 4.4A). To highlight the variability of the NCF frequency content, we calculate the standard deviations of the amplitude spectra for each frequency throughout the years (Figure 4.4B). The three maxima of the standard deviations at $T=5$ s, 8 s and 10 s mark the three period bands with the strongest temporal variations (three colored squares in Figure 4.4B). To further examine the phases of these variations, the time series of these three periods' amplitude spectra are displayed in Figure 4.4C. They all show very strong seasonality, which is also supported by the dominant 1-year peaks in period analyses of all frequencies' amplitude spectra time series (Figure 4.4D). Among the three periods with the largest variations, the $T=5$ s band is stronger in summer and weaker in winter by more than 50%, while the $T=10$ s band shows the opposite trend. This means that although the absolute raw noise level is lower in summer for Southern California, the

steps of pre-processing and calculating NCFs, including the temporal normalization and spectral whitening, do not remove the frequency content change of the raw noise, but produce the seesaw-style oscillating NCF amplitude spectrum. As pointed out by Tsai and Moschetti (2010), this is probably due to the presence of incoherent noise in the raw noise record. While the processing including spectral whitening is applied to the whole noise, cross correlations and NCFs only highlight the coherent part, whose spectrum is still not flat. Depending on the fraction of coherent noise and incoherent noise, the final NCFs may have the temporal variations of frequency content as observed (Figure 4.4).

With the more realistic oscillating NCF spectrum as observed in the LA Basin, we conduct a similar numerical test of apparent velocity change as in section 4.3 with the same phase spectrum but different amplitude spectra. As shown in Figure 4.5A, we set the reference NCF amplitude spectrum $A_r(\omega)$ to be the average NCF amplitude spectrum in winter, and set the current NCF amplitude spectrum $A_c(\omega)$ to be the average NCF amplitude spectrum in summer (see also Figure 4.4 for comparison). As previously described, the $A_c(\omega)$ spectrum has more high frequency energy. The resulting apparent velocity change $\varepsilon_{max}(t_0)$ as shown in Figure 4.5B has a similar shape to, but smaller amplitude than Figure 4.1B. It causes 0.05% apparent velocity increase up to $t_0 = 30$ s and the maximum cross correlation coefficients are all larger than 0.9. These values are comparable to observations made by Meier et al. (2010). Since the distance between station WTT and LCG is about 12 km, wavelets with $t_0 = 30$ s are well within the coda-wave window defined by most studies that assume a minimum velocity of 1 km/s (e.g., Meier et al. 2010). Additional numerical tests were also performed on smoother synthetic amplitude spectra with similar results as long as the fractional changes in spectra were comparable. In most real data applications, the stretching method is applied to NCF coda waves that consist of a series of scattered wavelets. In this study, we have chosen to examine each individual

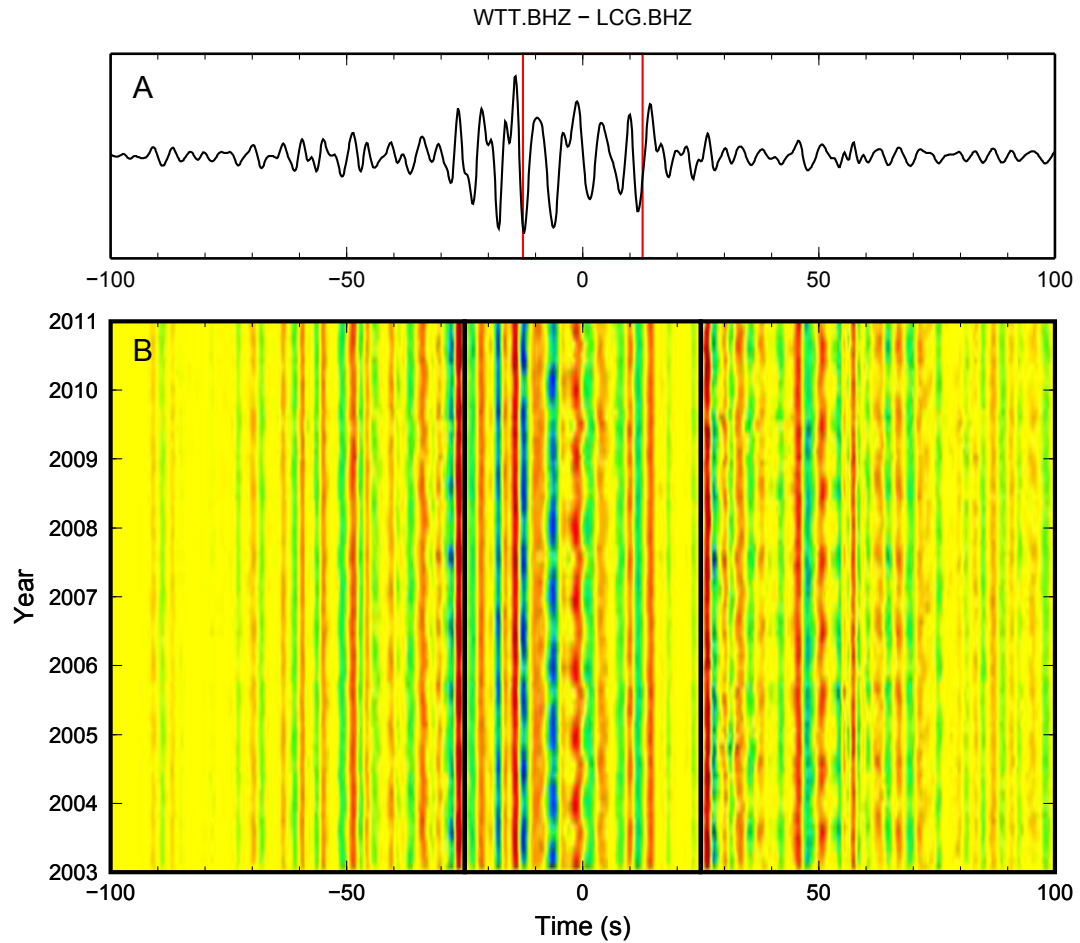


Figure 4.3: Noise cross correlation functions between WTT and LCG. (A) The stacked NCF between 2003 and 2011. The red lines mark the travel times for a wave speed of 1 km/s. Due to the shallow sediment layer, the direct wave-train lasts longer, corresponding to a wave speed of about 0.5 km/s. (B) The NCFs stacked every 60 days with 30 days overlapping show good signal-to-noise ratios and high coherence. Slight seasonal variations of the NCF waveforms can be observed. Different color-scales are used for direct waves and coda waves to highlight waveform details.

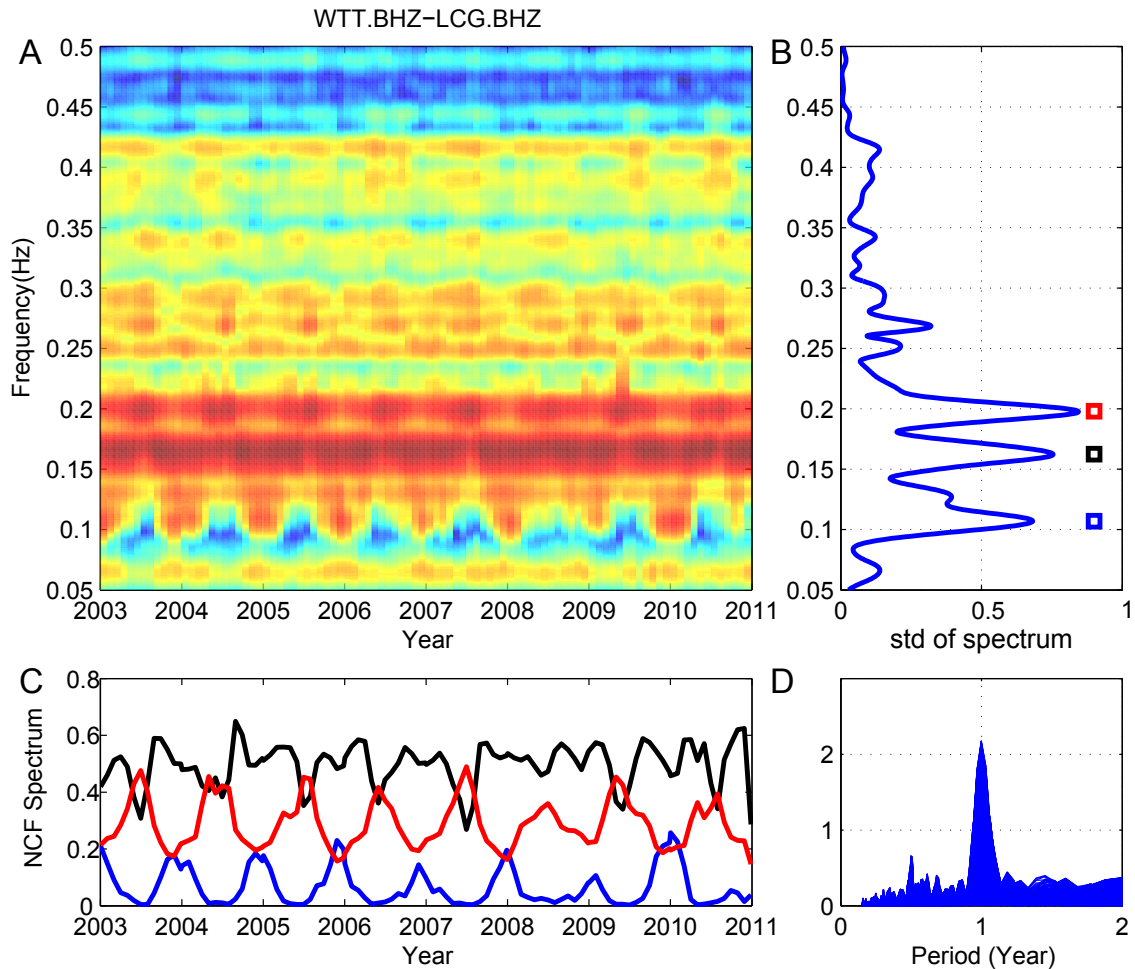


Figure 4.4: Temporal variability of NCF frequency content. (A) Amplitude spectra of the 60-day NCFs between 2003 and 2011 show clear seasonal patterns. (B) Standard deviation of the temporal variation of the NCF spectrum for each frequency. The three colored squares at the maxima mark the three period bands with the strongest temporal variations, and the corresponding time series of amplitude spectra are shown in (C) with different colors, respectively. (D) displays period analyses for all frequencies' temporal variations of amplitude spectra.

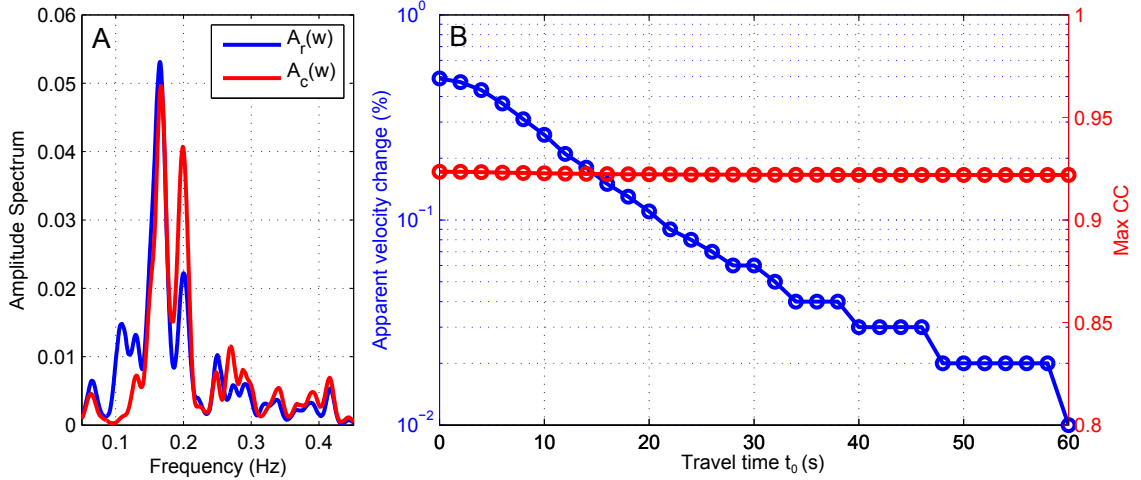


Figure 4.5: Similar numerical test of apparent velocity change $\varepsilon_{max}(t_0)$ as in Figure 4.1, but with the realistic NCF amplitude spectrum from the Los Angeles Basin. (A) The reference and current NCF amplitude spectra, $A_r(\omega)$ and $A_c(\omega)$ are set to be the average WTT-LCG NCF spectra in winter and summer, respectively. Note that $A_c(\omega)$ has more high frequency energy. (B) The blue line indicates the apparent velocity change $\varepsilon_{max}(t_0)$ calculated numerically using the stretching method. The red line shows the corresponding maximum cross correlation coefficients between the reference and current waveforms. Note that at $t_0 = 30$ s, the relative velocity change is 0.05%, comparable to the values measured in the Los Angeles Basin by Meier et al. (2010), and the maximum correlation value is >0.9 .

wavelet at different travel times, rather than the combined coda, because it is easier to understand the bias effect for an individual wavelet and the effect on the whole coda can be understood by combining the individual wavelet results. We also note that for the same change in amplitude spectra, our results are the same, whether these changes occur seasonal, daily, or of any other time scale.

The numerical tests also suggest potential ways to diagnose this bias due to change in frequency content. As shown in Figure 4.1B and 4.5B, the apparent velocity change $\varepsilon_{max}(t_0)$ decays with increasing t_0 , which means that, for a single NCF, the late part of the NCFs will produce smaller relative velocity changes. This trend is the opposite of what is expected from real velocity changes because late arrivals are more sensitive with more accumulated effect (Snieder et al., 2002; Brenguier et al., 2008a). The decay of $\varepsilon_{max}(t_0)$ with increasing t_0 also predicts that longer station pairs have smaller

relative velocity changes than closer pairs, also opposite to the expectation from real velocity changes. This seems to have been observed in the LA basin by Meier et al. (2010), where the observed seasonal velocity variations are only obvious at station pairs shorter than 30 km, and decays with increasing station pair distance. Meier et al. (2010) attribute this observation to lower NCF coherence at larger distances and reject the effect of variable noise sources by averaging over different time windows and station pairs with different azimuths. However, our numerical tests show that the bias due to change of frequency content is systematic for different time windows (t_0). As long as noise from different azimuths have similar trends in the temporal variations of frequency content (e.g., more high frequency noise in summer than in winter), which is a weak constraint, the bias is also systematic over all azimuths. This implies that the apparent velocity change cannot be diagnosed by taking averages of ε_{max} measured from different station pairs and different time windows.

4.5 Conclusions

We have shown that the temporal variability of NCF frequency content causes apparent velocity changes if the stretching method is used to measure the time shifts. This is primarily due to the mixing effects that stretching has on amplitude and phase spectra, and hence on waveform correlation. The apparent velocity change depends on a few factors: dispersion, forms of amplitude spectra, and travel times of time windows. Our numerical tests show that the bias decays with travel time, and therefore is most severe for close station pairs and early parts of the NCFs. For realistic seasonal variability of frequency content in the LA Basin and travel times up to 30s, our test examples still produce 0.05% apparent velocity changes and >0.9 waveform correlation coefficients, comparable to what usually has been observed in previous passive monitoring studies. Since temporal variability of noise frequency content at

different time scales can also be caused by the change of background seismic activity that accompanies major earthquakes, slow slip events (SSEs) or volcanic eruptions, it is important to check for this potential bias in future applications of passive monitoring. To diagnose this bias, time shifts measured from NCFs should be examined for dependence on travel times of time windows and distances of station pairs. The traditional cross-spectral doublet method may be free of this bias due to the separation of amplitude and phase spectra in the frequency domain before measuring time shifts.

Acknowledgments

We thank Fan-Chi Lin and Dongzhou Zhang for helpful discussions. We thank the editor Michael Ritzwoller and two anonymous reviewers for their comments that improved the manuscript. The facilities of the Southern California Earthquake Data Center (SCEDC), and the Southern California Seismic Network (SCSN), were used for access to waveforms data required in this study. This work is partially supported by the NSF/EAR-0838247 and Southern California Earthquake Center (12064).

References

- Aster, R.C., McNamara, D.E., Bromirski, P.D., 2008. Multidecadal climate-induced variability in microseisms. *Seismological Research Letters* 79, 194-202.
- Bensen, G.D., Ritzwoller, M.H., Barmin, M.P., Levshin, A.L., Lin, F., Moschetti, M.P., Shapiro, N.M., Yang, Y., 2007. Processing seismic ambient noise data to obtain reliable broad-band surface wave dispersion measurements. *Geophysical Journal International* 169, 1239-1260.
- Brenguier, F., Campillo, M., Hadziioannou, C., Shapiro, N.M., Nadeau, R.M., Larose,

- E., 2008a. Postseismic relaxation along the San Andreas fault at Parkfield from continuous seismological observations. *Science* 321, 1478-1481.
- Brenguier, F., Shapiro, N.M., Campillo, M., Ferrazzini, V., Duputel, Z., Coutant, O., Nercessian, A., 2008b. Towards forecasting volcanic eruptions using seismic noise. *Nature Geoscience* 1, 126-130.
- Clarke, D., Zaccarelli, L., Shapiro, N., Brenguier, F., 2011. Assessment of resolution and accuracy of the Moving Window Cross Spectral technique for monitoring crustal temporal variations using ambient seismic noise. *Geophysical Journal International* 186, 867-882.
- Duputel, Z., Ferrazzini, V., Brenguier, F., Shapiro, N., Campillo, M., Nercessian, A., 2009. Real time monitoring of relative velocity changes using ambient seismic noise at the Piton de la Fournaise volcano (La Réunion) from January 2006 to June 2007. *Journal of Volcanology and Geothermal Research* 184, 164-173.
- Grêt, A., Snieder, R., Aster, R.C., Kyle, P.R., 2005. Monitoring rapid temporal change in a volcano with coda wave interferometry. *Geophysical Research Letters* 32, L06304.
- Hadziioannou, C., Larose, E., Coutant, O., Roux, P., Campillo, M., 2009. Stability of monitoring weak changes in multiply scattering media with ambient noise correlation: Laboratory experiments. *Journal of the Acoustical Society of America* 125, 3688-3695.
- Li, Y.-G., Vidale, J.E., Aki, K., Xu, F., Burdette, T., 1998. Evidence of shallow fault zone strengthening after the 1992 M7. 5 Landers, California, earthquake. *Science* 279, 217-219.
- McNamara, D.E., Buland, R.P., 2004. Ambient noise levels in the continental United States. *Bulletin of the Seismological Society of America* 94, 1517-1527.

- Meier, U., Shapiro, N.M., Brenguier, F., 2010. Detecting seasonal variations in seismic velocities within Los Angeles basin from correlations of ambient seismic noise. *Geophysical Journal International* 181, 985-996.
- Minato, S., Tsuji, T., Ohmi, S., Matsuoka, T., 2012. Monitoring seismic velocity change caused by the 2011 Tohoku-oki earthquake using ambient noise records. *Geophysical Research Letters* 39, L09309.
- Niu, F., Silver, P.G., Daley, T.M., Cheng, X., Majer, E.L., 2008. Preseismic velocity changes observed from active source monitoring at the Parkfield SAFOD drill site. *Nature* 454, 204-208.
- Niu, F., Silver, P.G., Nadeau, R.M., McEvilly, T.V., 2003. Migration of seismic scatterers associated with the 1993 Parkfield aseismic transient event. *Nature* 426, 544-548.
- Peng, Z., Ben-Zion, Y., 2006. Temporal changes of shallow seismic velocity around the Karadere-Düzce branch of the north Anatolian fault and strong ground motion. *Pure and Applied Geophysics* 163, 567-600.
- Peng, Z., Ben-Zion, Y., 2005. Spatiotemporal variations of crustal anisotropy from similar events in aftershocks of the 1999 M7. 4 Izmit and M7. 1 Düzce, Turkey, earthquake sequences. *Geophysical Journal International* 160, 1027-1043.
- Poupinet, G., Ellsworth, W., Frechet, J., 1984. Monitoring Velocity Variations in the Crust Using Earthquake Doublets: An Application to the Calaveras Fault, California. *Journal of Geophysical Research* 89, 5719-5731.
- Rivet, D., Campillo, M., Shapiro, N.M., Cruz-Atienza, V., Radiguet, M., Cotte, N., Kostoglodov, V., 2011. Seismic evidence of nonlinear crustal deformation during a large slow slip event in Mexico. *Geophysical Research Letters* 38, L08308.

- Rubinstein, J.L., Uchida, N., Beroza, G.C., 2007. Seismic velocity reductions caused by the 2003 Tokachi-Oki earthquake. *Journal of Geophysical Research* 112, B05315.
- Sens-Schonfelder, C., Wegler, U., 2006. Passive image interferometry and seasonal variations of seismic velocities at Merapi Volcano, Indonesia. *Geophysical Research Letters* 33.
- Snieder, R., Grêt, A., Douma, H., Scales, J., 2002. Coda wave interferometry for estimating nonlinear behavior in seismic velocity. *Science* 295, 2253-2255.
- Stehly, L., Campillo, M., Shapiro, N.M., 2006. A study of the seismic noise from its long-range correlation properties. *Journal of Geophysical Research-Solid Earth* 111.
- Tsai, V.C., 2011. A model for seasonal changes in GPS positions and seismic wave speeds due to thermoelastic and hydrologic variations. *Journal of Geophysical Research* 116, B04404.
- Tsai, V.C., Moschetti, M.P., 2010. An explicit relationship between time-domain noise correlation and spatial autocorrelation (SPAC) results. *Geophysical Journal International* 182, 454-460.
- Vidale, J.E., Li, Y.-G., 2003. Damage to the shallow Landers fault from the nearby Hector Mine earthquake. *Nature* 421, 524-526.
- Wang, B., Zhu, P., Chen, Y., Niu, F., Wang, B., 2008. Continuous subsurface velocity measurement with coda wave interferometry. *Journal of Geophysical Research* 113, B12313.
- Xu, Z.J., Song, X., 2009. Temporal changes of surface wave velocity associated with major Sumatra earthquakes from ambient noise correlation. *Proceedings of the National Academy of Sciences* 106, 14207-14212.

Zaccarelli, L., Shapiro, N., Faenza, L., Soldati, G., Michelini, A., 2011. Variations of crustal elastic properties during the 2009 L'Aquila earthquake inferred from cross-correlations of ambient seismic noise. *Geophysical Research Letters* 38, L24304.

Zhan, Z., Wei, S., Ni, S., Helmberger, D., 2011. Earthquake centroid locations using calibration from ambient seismic noise. *Bulletin of the Seismological Society of America* 101, 1438-1445.